6. Scattering of X-Rays by Very Small Bodies

6.1 Small-angle Diffuse Scattering

When monochromatic X-rays are passed through very small particles, normally of the order of 10 to 2,000 Å or through a body containing zones of non-uniform density of about this size, a diffuse scattering pattern generally results within a very small range of angles around the incident direction (Fig. 6.1). Since the scattering is dependent upon the geometrical structure of the minute inhomogeneous zones, it is possible to establish the size, shape, state of aggregation, etc. of the small particles by analysis of the scattering pattern. This scattering differs in principle from diffraction, but is sometimes accompanied by diffraction due to normal Bragg diffraction (Section 4.1) and characteristic long repeat distances which can occur at very small angles. Since it is frequently impossible to distinguish unambiguously between these two contributions the term "small-angle scattering" is generally applied, without distinction, to them both.

In this section we attempt no more than an elementary explanation of the principle, analytical methods, and applications of small-angle scattering in the strict sense. If considerations of space did not preclude it, it would still be out of place in what is intended as a primer for experimental workers: the difficult theory and considerable overlap with other X-ray experimental methods have led the authors to refer the reader, instead, to the literature cited and to suitable textbooks for details.

Small-angle scattering is produced by substances containing small zones of non-uniform density which may be linear, planar, or particulate. The phenomenon has a remarkably wide application to the measurement of small particles, particularly in comparison with other physical methods. Thus, the breadths of the Debye-Scherrer rings are used in well-known method for the investigation of crystalline powders, and measurement methods based on viscosity, light scattering, osmotic pressure, surface tension, centrifugation, and electron microscopy have all been widely used for colloids and high polymers. However, these methods are all to some extent limited by the necessity to prepare the sample: X-ray small-angle scattering, on the other hand, has the very important advantages that the sample may be liquid, solid, crystalline, amorphous, or a mixture of these, and may take the form

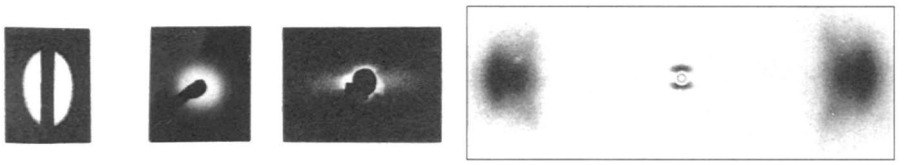

Fig. 6.1 X-ray small-angle scattering patterns. (a) With slit system, carbon black (*cf.* Fig. 15.1). (b) With pin-hole system. b_1) Polyethylene (undrawn), isotropic, central diffuse scattering. b_2) Curdlan(or β-(1→3)-D-Glucan), (draw direction vertical), diffuse scattering along the equator. b_3) Polyurethane, (draw direction vertical), merridional small-angle scattering and wide-angle diffractions on the equator. [Reproduced from K. Hess, H. Kiessig, cited by R. Hosemann, in "*Zur Struktur und Materie der Festkörper*", p.137, Deutsch. Mineral. Ges. (1951)]

of minute inclusions or voids. It also requires no special preparation of the sample, and is essentially non-destructive. Nevertheless, the method is not a simple panacea for all problems of small particle analysis: as with so many physical measurements, the legitimacy of an interpretation can only be established by checking very carefully the connection between theory and results (and the purpose for which they were obtained).

6.2 Small-angle Scattering Theory

The principles of X-ray small-angle scattering were established as early as 1930, and by about 1938, Guinier,[1] Kratky,[2] and Hosemann[3] had developed a quantitative treatment and shown how this scattering could be used. Further progress has been made since then as a result of various investigations into the problem of mutual interference based on differences between aggregations of particles, as well as into analytical methods and types of experimental equipment.

6.2.1 X-ray scattering by a substance of any structure

As summarized in Section 5.4, Eqs. 5.39 to 5.43 clearly show that, the central diffuse small-angle scattering is observed regardless the cohesive state of the substance, *i.e.* liquid, amorphous, crystalline, or paracrystalline, and in the case of crystalline or paracrystalline state the small-angle scattering is observed associated with each diffraction spot.

The other important conclusion obtained at the same time is that the intensity of the small-angle scattering depends upon the magnitude of $|<A>|^2$ (or $|F|^2$ for crystal or $<|F|>^2$ for paracrystal). This means that voids in substance can also give small-angle scattering as well as particles (Fig. 6.2).[4] Particle-like density heterogeneities in substances

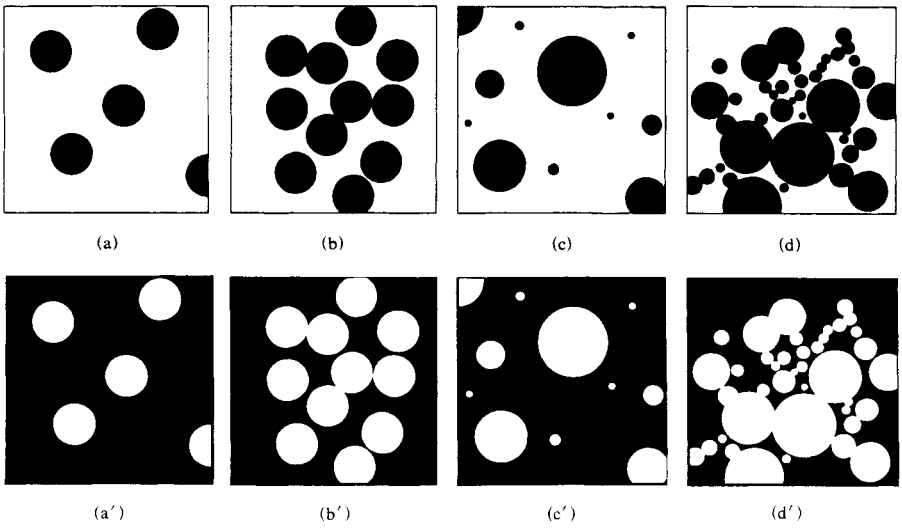

Fig. 6.2 Random assemblies of spherical particles.[4]
(a) Dilute system of identical particles; (b) Densely packed system of identical particles; (c) Dilute system of non-identical particles; (d) Densely packed system of non-identical particles.
(a′), (b′), (c′) and (d′) Complimentary system of (a), (b), (c) and (d), respectively.
[Reproduced with permission from *X-Ray Crystallography*, (I. Nitta ed.), Vol. II, p.519, Maruzen (1961)]

such as precipitation in alloys (Guinier-Preston zone) and inclusion in the matrix lattice of grain with a different lattice but with the same composition (Fig. 6.3[5]), also can give central diffuse small-angle scattering. Their intensities depend upon the electron density difference between void and matrix and that between the precipitation and matrix. This fact leads to the development of the "contrast variation method" (Section 6.2.2D).

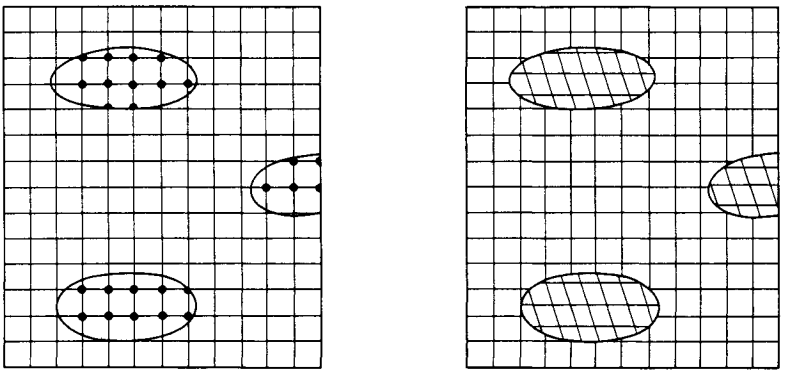

Fig. 6.3 Inhomogeneities in substance.[5]
(a) Precipitation of foreign atoms; clustered without lattice deformation.
(b) Inclusion in the matrix lattice of a grain with a different lattice but with the same composition.
[Reproduced from A. Guinier, G. Fournet, *Small-Angle Scattering of X-Rays*, p.201, John Wiley & Sons, Inc. (1955)]

6.2.2 Small-angle scattering from systems of dilutely dispersed particles (or voids)[6]

The small-angle scattering intensity by one particle with uniform density, ρ_∞ can be written as (*cf.* Eq. 5.14a)

$$I(\boldsymbol{S}) = I_e \rho_\infty \mid S(\boldsymbol{S}) \mid^2 \tag{6.1}$$

where the shape factor

$$S(\boldsymbol{S}) = \int_{particle} \exp(2\pi i(\boldsymbol{S}\cdot\boldsymbol{r}))\mathrm{d}v_r \tag{6.2}$$

and then

$$I(\boldsymbol{S}) = I_e \rho_\infty^2 \mid S(\boldsymbol{S}) \mid^2 = I_e \rho_\infty^2 V^2 \Psi(\boldsymbol{S}) = I_e n^2 \Psi(\boldsymbol{S}) \tag{6.3}$$

where $\mid S(\boldsymbol{S}) \mid^2 = V^2 \Psi(\boldsymbol{S})$, $\Psi(\boldsymbol{S})$ is the scattering function of the particle and $n(= V\rho_\infty)$ is the number of electrons in a particle, respectively.

If the shape of the particle is known as, for example, parallelepiped, sphere, ellipsoid of revolution, cylinder, etc. based on the theoretical equation for the three-dimensional particle shape, the scattering function can be obtained analytically or at least by numerical calculation. Some examples of the scattering functions are given below.

A. Globular particles

a) A globular particle fixed in a space.

1) A spherical particle of uniform density with radius R. This is the simplest case, and

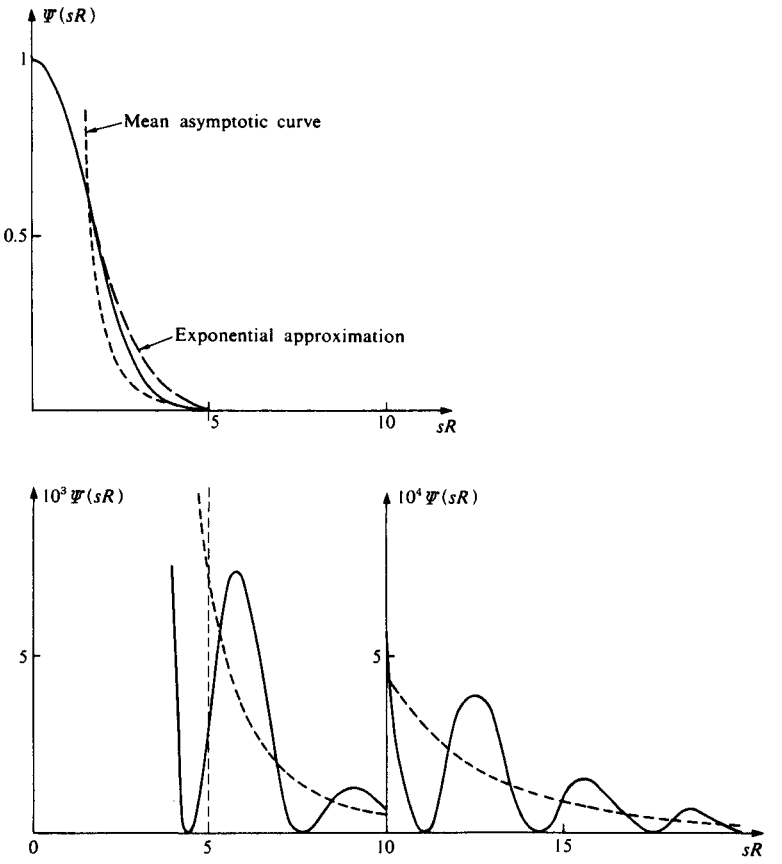

Fig. 6.4 Scattering intensity from a sphere of radius R, $\Psi(sR)$.[8]
The curve is drawn with different scales for the various ranges of sR ($\times 10^3$ for $4 < sR < 10$; $\times 10^4$ for $sR > 10$) ($s = 2\pi S$, $S = (2\sin\theta)/\lambda \fallingdotseq 2\theta/\lambda = \varepsilon/\lambda$).
Exponential approximation: $\exp\left\{\frac{-(sR)^2}{5}\right\}$; mean asymptotic curve: $\frac{9}{2}\frac{1}{(sR)^4}$.
[Reproduced from A. Guinier, G. Fournet, *Small-Angle Scattering of X-Rays*, p.20, John Wiley & Sons, Inc. (1955)]

the scattering function has been given by Rayleigh[7] (Fig. 6.4),

$$\Psi(S) = \Phi^2(2\pi SR)$$

$$= \left[3\frac{\sin(2\pi SR) - (2\pi SR)\cos(2\pi SR)}{(2\pi SR)^3}\right]^2 = \frac{9\pi}{2}\left[\frac{J_{3/2}(2\pi SR)}{(2\pi SR)^{3/2}}\right]^2 \qquad (6.4)$$

2) A rectangular parallelepiped with three edge lengths of a, b, and c.[6] We assume that the a, b, and c edges of the parallelepiped are parallel to the x, y, and z axes, respectively (Fig. 6.5), and that the y axis is parallel to, and the x and z axes perpendicular to the incident X-ray beam, and that three components of S, the ξ, η and ζ axes are parallel to the x, y, and z axes, respectively.

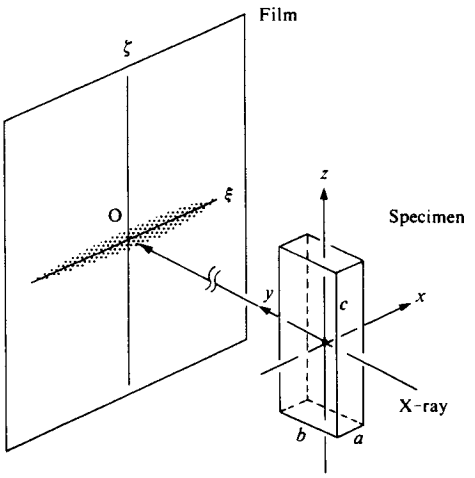

Fig. 6.5 Small-angle scattering from a fixed parallelepiped.

Then, the scattering function is given

$$\Psi(S)=\Psi(\xi,\eta,\zeta)=\frac{\sin^2(\pi\xi a)}{(\pi\xi a)^2}\cdot\frac{\sin^2(\pi\eta b)}{(\pi\eta b)^2}\cdot\frac{\sin^2(\pi\zeta c)}{(\pi\zeta c)^2} \tag{6.5}$$

This equation indicates that the diffuse small-angle scattering appears along the ξ, η and ζ directions with the broadening of $1/a$, $1/b$, and $1/c$, respectively. As the X-ray incidence is parallel to the y (or b) axis the scattering diagram observed corresponds to the $\xi\zeta$ section of $\Psi(S)$.

If the particle is a crystal, this small-angle scattering associates with all the reciprocal lattice points: the resultant is the Laue diffraction function (Eq. 2.38 and Fig. 5.12).

3) A globular particle with any shape at a fixed position (Guinier's approximation).[6]

In general, the shape of the particle is unknown or is so complicated that it is difficult to express its shape by analytical equation in order to obtain the scattering function. In such a case, the only information obtainable about the magnitude of the particle is the radius of gyration, R_g of the particle with respect to its center of gravity.

Taking the y axis again parallel to and the x and z axes perpendicular to the incident X-ray beam, and the origin at the center of gravity of the particle, the scattering observed on the xz plane is, since $\eta=\zeta=0$,

$$S(\xi,0,0)=\int\exp(2\pi i\xi x)\mathrm{d}x\mathrm{d}y\mathrm{d}z \tag{6.6}$$

As the scattering angle is small and therefore ξ is small, the exponential function in Eq. 6.6 can be expanded by a series,

$$S(\xi,0,0)=\int(1+2\pi i\xi x-2\pi^2\xi^2x^2+\ldots)\mathrm{d}x\mathrm{d}y\mathrm{d}z \tag{6.7}$$

The second term in Eq. 6.7 is zero by integration since the origin is taken at the center of gravity of the particle. If we write

$$R_x^2 = \frac{1}{V}\int x^2 \mathrm{d}x\mathrm{d}y\mathrm{d}z \tag{6.8}$$

the scattering intensity is

$$\begin{aligned} I(\xi, 0, 0) &= I_e\rho^2 |\, S(\xi, 0, 0)\,|^2 \\ &= I_e\rho^2\, V^2(1 - 2\pi^2 R_x^2\xi^2 + \ldots)^2 \\ &= I_e n^2 \exp(-4\pi^2 R_x^2\xi^2) \end{aligned} \tag{6.9}$$

and

$$\log I(\xi, 0, 0) = \log[I_e n^2] - 4\pi^2 R_x^2\xi^2 \tag{6.10}$$

The tangent of the log I *vs.* ξ^2 plot in the neighborhood of $\xi = 0$ gives the value of R_x and hence if the particle shape and the orientation of the particle with respect to the x and z axes is known the tangent gives an information on the particle size. (*cf.* Fig. 6.7 and also Table 5 in the Appendix).

b) Globular particles with random orientation.

1) Spherical particles with radius R. The scattering function $\Psi(S)$ shows no change from that given by Eq. 6.4, since the sphere shows no directional difference in shape, and the small-angle scattering intensity of a spherical particle is:[7]

$$\langle I(S)\rangle = I(S) = I_e n^2\, \Psi(S). \tag{6.11}$$

$$\Psi(S) = \left[3\frac{\sin(2\pi SR) - (2\pi SR)\cos(2\pi SR)}{(2\pi SR)^3}\right]^2$$

If the specimen is a dilute system consist of M identical particles the intensity given in the above equation must be multiplied by M.

$$\langle I(S)\rangle = I_e\, Mn^2\Psi(S) \tag{6.11a}$$

The scattering function $\Psi(2\pi SR)$ *vs.* $2\pi SR$ or $\Psi(sR)$ *vs.* sR (where, $s = 2\pi S$ and $S \doteqdot 2\theta/\lambda = \varepsilon/\lambda$ (for very small angles)) is shown in Fig. 6.4,[8] which is compared with its exponential approximations (*cf.* Fig. 15.5).

2) Ellipsoids of revolution with axial lengths of $2a$, $2a$, and $2wa$ (axial ratio $w = b/a$).[1]

$$\langle I(S)\rangle = I_e Mn^2 \int_0^{\pi/2} \psi(2\pi Sa\sqrt{(\cos^2\theta + w^2\sin^2\theta)}\,)\cos\theta \mathrm{d}\theta \tag{6.12}$$

The scattering curves for ellipsoids of revolution with various axial ratios w are shown in Fig. 6.6.[9] The log $I(S)$ *vs.* log S (or log $I(\varepsilon)$ *vs.* log ε, etc.) plot of the scattering curve (log-log plot) is often used to obtain a rough information on the overall shape of the particle (curve-fitting method *cf.* Section 15.2.2)

3) Globular particles with any shape. If the orientation of particles is not fixed, Eq. 6.7 must be averaged for all orientations of particles. The summation of the R_x^2 and its analogs along the y and z axes gives the square of R_g, the radius of gyration with respect to the center of gravity (Guinier's approximation).

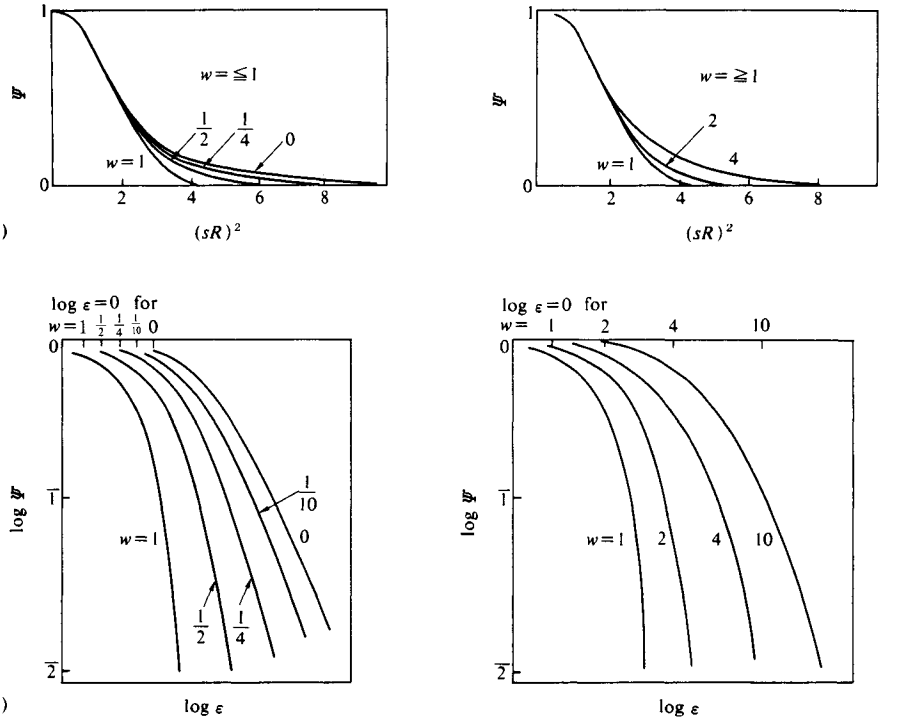

Fig. 6.6 Theoretical scattering curves for ellipsoids of revolution with various axial ratios w.[9] (a) Scattering function Ψ vs. $(sR)^2$, (b) Log-log plot derived from (a) where $sR = 2\pi SR = 2\pi\varepsilon R/\lambda$. [Reproduced from A. Guinier, *Ann. Phys. (Paris)*, **12**, 161, Masson et Cie. (1939)]

$$R_x^2+R_y^2+R_z^2=\frac{1}{V}\int(x^2+y^2+z^2)\mathrm{d}x\mathrm{d}y\mathrm{d}z = R_g^2 \tag{6.13}$$

For random orientation all the averages of R_x^2, R_y^2, and R_z^2 are equal, and $< R_x^2 >$ can be written equal to $R_g^2/3$.

$$< \Psi(S) > = \exp[-4\pi^2 R_g^2 S^2/3] \tag{6.14}$$

$$< I(S) > = I_e Mn^2 \exp[-4\pi^2 R_g^2 S^2/3] \tag{6.15}$$

$$\log < I(S) > = \log(I_e Mn^2) - 4\pi^2 R_g^2 S^2/3 \tag{6.16}$$

$$= \log[I(0)] - 4\pi^2 R_g^2 S^2/3 \tag{6.16a}$$

If we plot values of $\log I(S)$ against S^2 (experimentally, $\log I(\varepsilon)$ *vs.* ε^2; $\varepsilon = 2\theta$: scattering angle) we can obtain a straight line in a small S (or ε) region[1] (Guinier plot, Fig. 6.7), and we can easily determine the value of R_g from its slope, α ($= -4\pi^2 R_g^2/3\lambda^2$) (Section 15.2). If the shape of the particles is known, information about the particle size will be obtained.

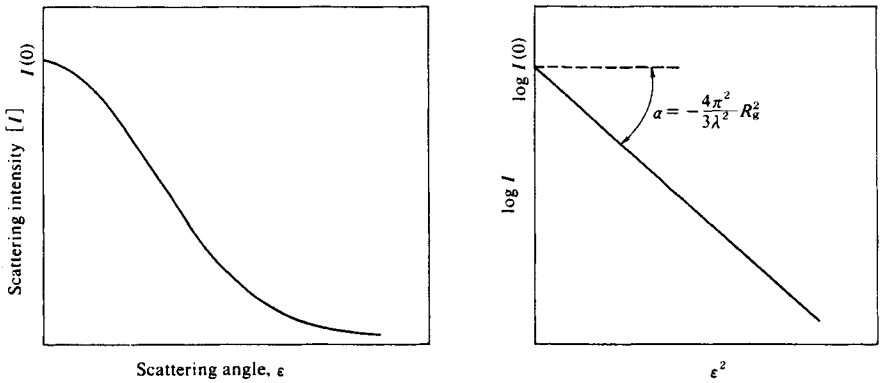

(a) $I = I(0)\exp\left(-\frac{4\pi^2}{3\lambda^2}R_g^2\varepsilon^2\right)$ (b) $\log I = \log I(0) - \frac{4\pi^2}{3\lambda^2}R_g^2\varepsilon^2$

Fig. 6.7 Small-angle scattering curve and Guinier plot (ε: scattering angle).

B. Rod-like particles [6]

a) A rod-like particle fixed in a space. If the long axis of the rod (length H) is parallel to the z axis (*cf.* Fig. 6.5), the scattering function is

$$S(\xi,\eta,\zeta) = \iiint_{\text{section}} \int_{-\frac{H}{2}}^{\frac{H}{2}} \exp[2\pi i(\xi x+\eta y+\zeta z)]\mathrm{d}x\mathrm{d}y\mathrm{d}z$$

$$= \frac{\sin(\pi H\zeta)}{\pi L\xi}\iint \exp[2\pi i(\xi x+\eta y)]\mathrm{d}x\mathrm{d}y \tag{6.17}$$

For the scattering observed on the $\xi\zeta$ plane, $\eta = 0$, and by the approximation for the small-angle Eq. 6.17 can be written as

$$S(\xi,0,\zeta) = H\frac{\sin(\pi H\zeta)}{\pi H\zeta}\iint \exp[2\pi i\xi x]\mathrm{d}x\mathrm{d}y$$

$$= HA\frac{\sin(\pi H\zeta)}{\pi H\zeta}\exp[-2\pi^2\xi^2 R_{xq}{}^2] \tag{6.18}$$

and then

$$I(\xi,\zeta) = I_e M n^2 \frac{\sin^2(\pi H\zeta)}{(\pi H\zeta)^2}\exp[-4\pi^2\xi^2 R_{xq}{}^2] \tag{6.19}$$

where, A is the transverse sectional area of the rod, $V = HA$, and

$$R_{xq}{}^2 = \frac{1}{A}\iint x^2\mathrm{d}x\mathrm{d}z \tag{6.20}$$

If H is large (*i.e.* the rod is long), the small-angle scattering intensity concentrates in the neighborhood of the ζ axis to give a streak along the ξ axis, of which the integral breadth is $1/H$.

b) Identical rod-like particles, of which all the long axes are parallel to the z axis but their transverse sections are randomly oriented.

Average R_{xq}^2 is

$$< R_{xq}^2 > = R_{gs}^2/2 \tag{6.21}$$

where, R_{gs} = is the radius of gyration of the section perpendicular to the long axis of the rod, and

$$R_s^2 = \frac{1}{A}\int (x^2+y^2)\mathrm{d}x\mathrm{d}y \tag{6.22}$$

and the small-angle scattering intensity on the ζ axis is

$$I(S) = I_e\, Mn^2 \exp[-2\pi^2 S^2 R_{gs}^2] \tag{6.23}$$

$$\log I(S) = \log[I_e\, Mn^2] - 2\pi^2 S^2 R_{gs}^2 \tag{6.24}$$

The Guinier plot of the equatorial small-angle scattering gives the radius of gyration of the section, R_{gs} of the rod-like particle (*cf.* Fig. 6.8(a) and Section 15.2.2).

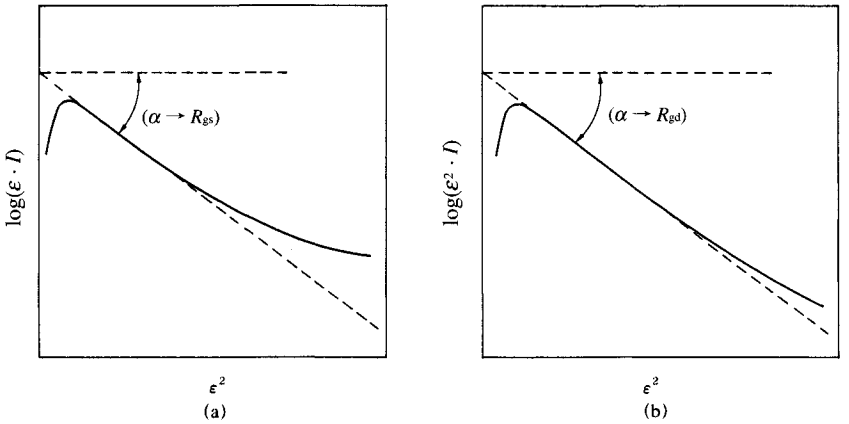

Fig. 6.8 Guinier plot of $\log(\varepsilon \cdot I)(= \log I_{BT})$ *vs.* ε^2 for R_{gs} and $\log(\varepsilon^2 \cdot I)$ *vs.* ε^2 for R_{gd}.

c) Randomly oriented rod-like particles (1/H ≪ S ≪ 1/R, H: length, R: radius of the section).

1) General case.

The scattering intensity concentrated on the $\xi\eta$ plane (Fig. 6.5) is dispersed for all directions and the intensity given by Eq. 6.23 is weakened by the factor $1/(2SH)$

$$< I(S) > = I_e Mn^2 \frac{1}{2SH} \exp[-2\pi^2 R_{gs}^2 S^2] \tag{6.25}$$

and

$$\log[S < I(S) >] = \text{Const.} - 2\pi^2 R_{gs}^2 S^2 \tag{6.26}$$

As special cases, the scattering intensities from uniform cylindrical particles and from rods of infinitesimal transverse dimensions are given in the following formulae.

2) Cylinders of revolution of diameter $2R$ and length H[10)]

$$<I(S)> = I_e M n^2 \int_0^{\pi/2} \frac{\sin^2(\pi SH\cos\theta)}{(\pi SH\cos\theta)^2} \cdot \frac{4J_1^2(2\pi SR\sin\theta)}{(2\pi SR\sin\theta)^2} \sin\theta d\theta \tag{6.27}$$

3) Fibers of extremely small radius and length H[10–12)]

$$<I(S)> = I_e M n^2 \left[\frac{Si(2\pi SH)}{\pi SH} - \frac{\sin^2(\pi SH)}{(\pi SH)^2} \right] \tag{6.28}$$

where

$$Si(x) = \int_0^x \frac{\sin t}{t} dt.$$

C. Disc-shaped particle ($1/H \gg S \gg 1/R$)[6)]

The scattering intensity concentrate in the direction perpendicular to the disc plane.

a) A disc-shaped particle fixed in a space.

If the disc plane is parallel to the x axis, assuming that $\xi = 0$ in Eq. 6.19

$$I(\zeta) = I_e M n^2 \frac{\sin^2(\pi H\zeta)}{(\pi H\zeta)^2} \tag{6.29}$$

$$= I_e M n^2 \exp[-\pi^2 H^2 \zeta^2/3] \tag{6.30}$$

b) Randomly oriented disc-shaped particles. For random orientation, the exact form of the small-angle scattering intensity from the flat disc of infinitesimal thickness and diameter $2R$ is given[13)]

$$<I(S)> = I_e M n^2 \frac{2}{(2\pi SR)^2} \left[1 - \frac{1}{2\pi SR} J_1(2\pi SR) \right] \tag{6.31}$$

That is, the scattering intensity to be concentrated on the ξ axis is weakened by the factor $1/S^2$, and $\log[S^2 I(S)]$ *vs.* S^2 (or $\varepsilon^2 I(\varepsilon)$ *vs.* ε^2) plot becomes linear, from its slope we can de-

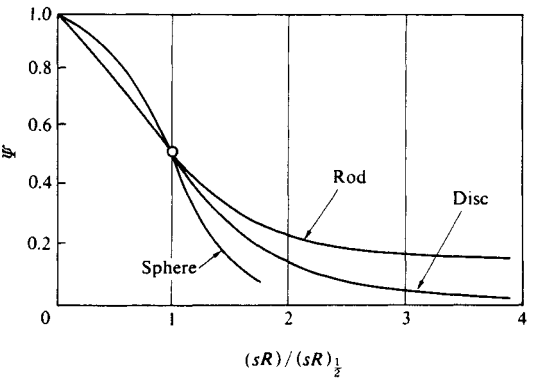

Fig. 6.9 Theoretical scattering curves for spherical, disc-shaped, and rod-like particles[9)].
R is the radius of the sphere, the diameter of the disc, or the length of the rod. The abscissa is transformed as $(sR)/(sR)_{1/2}$ so that all three curves pass through the same point, which is defined as the point where the scattering function has exactly half its maximum value. ($sR = 2\pi SR = 2\pi\varepsilon R/\lambda$)
[Reproduced from O. Kratky, G. Porod, *J. Colloid Sci.*, **4**, 35, Academic Press (1949)]

termine the thickness of the disc H (Fig. 6.8(b) and *cf.* Section 15.2.2B).

In Fig. 6.9 the scattering curves for spherical, rod-like and disc-shaped particles are compared.[9]

If we assume the overall shape of the particle to be a hollow sphere, cylinder, hollow cylinder, rod or other, and if we can calculate the scattering functions numerically, we can apply the curve-fitting method (log-log plot) to simulate the most suitable shape and size of the particle.

D. Particles suspended in a medium

If the particles are dispersed within a suspending medium and the particles are impermeable, the number of electrons n in Eq. 6.11 and other equations in the preceding sections must be replaced by the product of the difference $\Delta\rho = \rho_1 - \rho_2$ between the electron densities in the two phases and the volume of the particles V_1, *i.e.* by the effective electron excess or deficiency $\Delta\rho\ V_1$ in the particles.

$$< I(S) > = I_e\, M(\Delta\rho\ V_1)^2\, \Psi(S) \tag{6.32}$$

This means that increasing the electron density outside V_1 is equivalent to decreasing the scattering intensity uniformly within the particle. In the early times Barton and Brill[14] confirmed this fact experimentally for the small-angle scattering from carbon black suspended in aqueous solutions of inorganic salt by changing the concentration of salt.

a) Contrast variation method.[15–18] To obtain more information on the structure of inhomogeneous particles the contrast variation method is often used, especially in the field of neutron small-angle scattering. This method uses solvents of different electron densities.

The contrast $< \Delta\rho >$ is the mean difference in scattering density between the particle ρ_1 and solvent ρ_2.

$$< \Delta\rho > = \bar{\rho}_1 - \bar{\rho}_2 \tag{6.33}$$

where $\bar{\rho}_1$ and $\bar{\rho}_2$ are averages of ρ_1 and ρ_2 over the volume V_1, respectively.

If we assume that within the volume V_1 of the particle the electron density remains unchanged while the surrounding solvent has a variable homogeneous electron density ρ^2, the difference in electron density is then assumed to be the sum of the two terms. One describes the effect of excluding solvent from the region occupied by the particle; this term is directly affected by the contrast between the particle and solvent. The other term covers any variation within the particle (Fig. 6.10).

$$< \Delta\rho(r) > = < \Delta\rho > \sigma_1(r) + \rho_3(r) \tag{6.34}$$

$\sigma_1(r) = 1$ inside the particle and zero outside. Thus, $\int \sigma_1(r)\mathrm{d}r = V_1$. The ρ_3 is the deviation from the mean difference electron density $< \rho >$: it arises from any internal structure within the particle. It further holds that

$$\int_{V_1} \rho_3(r)\mathrm{d}r = 0 \tag{6.35}$$

The scattering amplitude of the particle is calculated as

$$A(S) = < \rho > S_1(S) + A_3(S) \tag{6.36}$$

where $S_1(S)$ and $A_3(S)$ are the Fourier transforms of $\sigma_1(r)$ and $\rho_3(r)$, respectively. The scattering intensity is

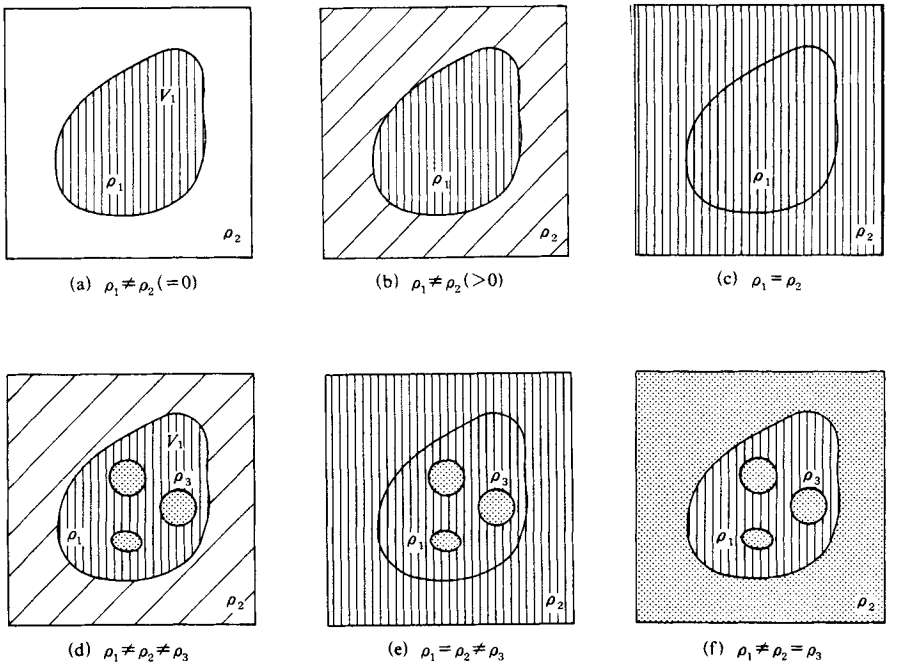

Fig. 6.10 Effect of the contrast.
V_1 denotes the volume of a particle; ρ_1, ρ_2 and ρ_3 are the densities of a particle, of the dispersion medium and of internal inhomogeneity in the particle, respectively,
(a) $\rho_1 \neq \rho_2 (=0)$, particle with uniform density in vacuum; (b) $\rho_1 \neq \rho_2 (>0)$, particle with uniform density in a medium. A similar but less intense small-angle scattering(a) is observed; (c) $\rho_1 = \rho_2$, particle has the same density as the medium. No small-angle scattering is observed; (d) $\rho_1 \neq \rho_2 \neq \rho_3$, particle which has internal inhomogeneity in a medium; (e) $\rho_1 = \rho_2 \neq \rho_3$. Only internal inhomogeneities with density ρ_3 give small-angle scattering; (f) $\rho_1 \neq \rho_2 = \rho_3$. Only inhomogeneity ρ_1 gives small-angle scattering.

$$I(S) = A(S)A*(S)$$
$$= <\Delta\rho>^2 |S_1(S)|^2 + <\Delta\rho> |S_1(S)A_3(S)| + |A_3(S)|^2 \tag{6.37}$$

In Eq. 6.37, $|S_1(S)|^2$ is the "shape factor" of the volume V_1 and can be determined by extrapolation because $A_3(S)$ vanishes at $S = 0$. The square root of the scattering intensity at zero angle is linear in $<\Delta\rho>$; and $[I(0)]^{1/2} = <\Delta\rho> |S_1(0)|$. $|A_3(S)|^2$ originates from $\rho_3(r)$ and is measurable if $<\Delta\rho> = 0$. $|A_3(S)|^2 = 0$ according to Eq. 6.35. The cross term $|S_1(S)A_3(S)|$ establishes the correlation between $|S_1(S)|^2$ and $|A_3(S)|^2$ by the following general inequality

$$|S_1(S)A_3(S)| \leqq \frac{1}{2}\sqrt{|S_1(S)|^2 \cdot |A_3(S)|^2} \tag{6.38}$$

Introduction of Eq. 6.34 into the definition of the radius of gyration R_g yields

$$R_g^2 = R_3^2 + \alpha/<\Delta\rho> - \beta/<\Delta\rho>^2 \tag{6.39}$$

where

$$R_3^2 = \frac{1}{V_1}\sigma_1(r)r^2\mathrm{d}r \tag{6.40}$$

$$\alpha = \frac{1}{V_1}\rho_3 r^2\mathrm{d}r \tag{6.41}$$

$$\beta = \frac{1}{V_1}\rho_3(r)\rho_3(r')\cdot r\cdot r'\mathrm{d}r\mathrm{d}r' \tag{6.42}$$

R_3 represents the radius of gyration of a homogeneous particle and does not depend on $<\Delta\rho>$. α is the second moment of the electron density fluctuations. If the sign of α is positive the positive contributions dominate. β is an asymmetry parameter according to Eq. 6.40. The R_g^2 *vs.* $1/<\Delta\rho>$ is a straight line if $\beta = 0$, and the slope of this line is α and the value of R_g^2 at $1/<\Delta\rho> = 0$ is R_s^2.

The contrast variation method for X-ray small-angle scattering is performed by variations in the concentration of sugar or other low molecular weight solutes. Difficulties may arise from preferential interactions between solvent components and the macromolecule under investigation.

E. S^{-4} Rule of scattering intensity

As shown earlier the small-angle scattering intensity of a system of spherical particles of radius R and density ρ is given by Eq. 6.11, which can be written as follows as

$$n^2 = (\rho V)^2 = (4/3\cdot\pi R^3\rho)^2.$$

$$I(S) = \frac{\rho^2}{8\pi^3}\left[\frac{4\pi R^2}{S^4} + \frac{1}{\pi S^6} - \frac{4R}{S^5}\sin(4\pi SR) - \frac{4R^2}{S^4} - \frac{1}{\pi S^6}\cos(4\pi SR)\right] \tag{6.43}$$

For sufficiently large S, the second and higher terms in the bracket can be neglected and

$$I(S) = \frac{\rho^2}{8\pi^3}\cdot\frac{4R^2}{S^4} \tag{6.44}$$

This means that theoretically the tail end (or fmal slope) of the small-angle scattering curve should conform to the asymptotic course for S^{-4}.[19]

For the two-phase system the asymptotic value of $S^4I(S)$ is rational to the square of density difference and the area of the interface.

$$\lim_{S\to\infty} S^4 I(S) = \frac{1}{8\pi^2}(\rho_1-\rho_2)\cdot(\text{Area of the interface}) \tag{6.45}$$

6.2.3 Correlation function and distance distribution function[20,21]

A. Correlation function

a) Dilute particle system. The particles are randomly oriented and far from each other so that all the interparticle interference may be neglected. The scattering intensity is given

$$<I(S)> = \rho^2 V\int_0^\infty \gamma_0(r)\frac{\sin Sr}{Sr}4\pi r^2\mathrm{d}r \tag{6.46}$$

where $\gamma_0(r)$, the correlation function[22,23] (characteristic function[19] or distance probability function) of the particle, represents the probability that a point at a distance r in an arbitrary

direction from a given point in the particle will itself also be in the particle (See Fig. 5.8).

The properties of $\gamma_0(r)$ are: from the definition $\gamma_0(0)=1$ and γ_0 decreases as r increases. It becomes zero when r is greater than the maximum particle diameter.

$$\int_0^\infty 4\pi r^2\gamma_0(r)\mathrm{d}r = V = \frac{4\pi}{\rho^2}\int_0^\infty S^2 I(S)\mathrm{d}S, \tag{6.47}$$

and

$$\int_0^\infty \gamma_0(r)\mathrm{d}r = \frac{<l>}{2} = \frac{\pi}{\rho^2 V}\int_0^\infty S<I(S)>\mathrm{d}S \tag{6.48}$$

$<l>$ is the average of the diameters drawn through every point within the particle in all directions.

$$\left.\frac{\mathrm{d}\gamma_0}{\mathrm{d}r}\right|_{r\to 0} = \frac{O}{4V} \tag{6.49}$$

where O is the surface area of the particle. This relation is a consequence of the fact $S^4<I(S)>$ must tend toward a constant limiting value

$$\lim S^4<I(S)> = \frac{\rho^2 O}{8\pi^3} \tag{6.50}$$

as S increases.

By Fourier inversion the correlation function γ_0 is obtained from the small-angle scattering intensity measured.

$$\gamma_0(r) = \frac{2}{\rho^2 V r}\int_0^\infty S<I(S)>\sin 2\pi r S\mathrm{d}S \tag{6.51}$$

b) General case. The specimen composed of matter of uniform electron density ρ filling a fraction χ_1 of the total volume V_0 is

$$I(S) = V_0\rho^2\chi_1\chi_2\int_0^\infty \gamma(r)\frac{\sin 2\pi Sr}{2\pi Sr}4\pi r^2\mathrm{d}r \tag{6.52}$$

where $\chi_2 = 1-\chi_1$, $\gamma(r)$ is the correlation function of the heterogeneous system, and for a system composed of identical particles $\gamma(r)$ becomes $\gamma_0(r)$, the correlation function of the particle. In the general case $\gamma(r)$ is defined in the following way: Let $Y(r)$ be the probability that a point a distance r from another point occupied by matter is also occupied by matter.

Then

$$Y(r) = \chi_1 + \chi_2\gamma(r)$$

By Fourier inversion $\gamma(r)$ may be obtained from the experimental data.

The limit of the product $S^4 I(S)$ is still given by $(\rho^2/8\pi^3)O_0$. (O_0: total surface area).

B. Distance distribution function[24]

a) Globular particles. Using the correlation function the distance distribution function of the particle is defined as

$$p(r) = \gamma_0(r)\cdot r^2. \tag{6.53}$$

$4\pi p(r)$ represents the number of lines with lengths r, which are found in the combination of any volume element j with any other volume element k.

Inhomogeneous particles may have regions with positive and negative contributions to the $p(r)$.

1) Sphere. The distance distribution function of a sphere is given analytically.[20]

$$p(r) = \text{const.} \cdot x^2(2 - 3x + x^3) \tag{6.54}$$

where $x = r/2R$ and R is the radius of the sphere. The maximum of the $p(r)$ is near $r = R(x = 0.5)$ (Fig. 6.11). Any deviation from spherical symmetry shifts the maximum to smaller r values if R is kept constant.

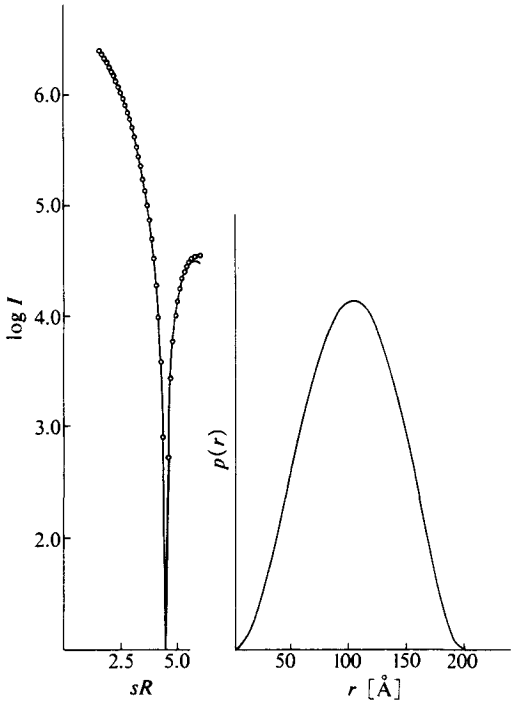

Fig. 6.11 Theoretical scattering function of a sphere (R=100Å, log I *vs.* sR plot) and theoretical distance distribution, $p(r)$.[21] [Reproduced with permission from I. Pilz *et al.*, *Methods in Enzymology*, **61**, 168, Academic Press (1980)]

2) Particles elongated in one direction which have a constant cross section of arbitrary shape. In this case, such as long cylinders and prisms, the $p(r)$ show a linear decrease at large r values (Fig. 6.12). The maximum dimension of the cross section d_{max} is much smaller than that of the particle.

$$2R/d_{max} \geqq 2.5 \tag{6.55}$$

The slope of the linear region is given by

$$\tan\alpha = -\frac{dp}{dr} = \frac{A^2 < \rho_c >^2}{2\pi} \tag{6.56}$$

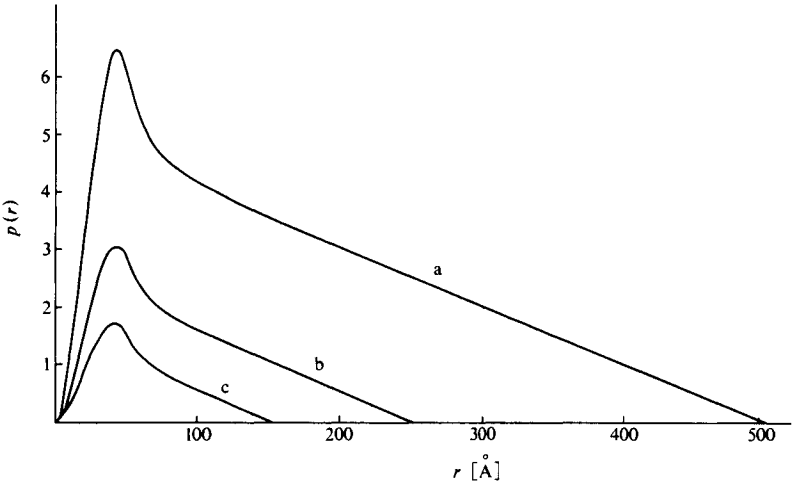

Fig. 6.12 Distance distributions from homogeneous prisms with edge lengths of (a) 50:50:500, (b) 50:50:250, (c) 50:50:150.[21]
[Reproduced with permission from I. Pilz *et al.*, *Methods in Enzymology*, **61**, 169, Academic Press (1980)]

A is the area of the cross section and

$$\rho_c = \frac{1}{A}\int_A \rho_c(x)\mathrm{d}a \tag{6.57}$$

where $\rho_c(x)$ is the electron density in the cross section. Difference in the area of the cross section results in a pronounced difference in the slope from α according to Eq. 6.56.

3) Lamellar particles. In this case, the number of distances in a plane is equal to $2\pi r\gamma_0(r)$. In analogy to the distance distribution of the whole particle $p(r)$, we define the distance distribution of a plane with

$$P_L(r) = \gamma_0(r)r = p(r)/r \tag{6.58}$$

The $p_L(r)$ functions of lamellar particles with the same plane and different thickness t are given in Fig. 6.13. They start at $r = 0$ and show a rapid increase, and at a point near $r = t$ begin to decrease almost linearly. The limiting value A_L, of the $p_L(r)$ function resulting from the extrapolation of this quasi-linear part toward $r = 0$ contains information on the area of the basal plane of the lamella.

$$A_L = p_L(r)\Big|_{r\to 0} = \frac{<\rho_t>^{-2} At^2}{2} = \frac{<\rho_t>^{-2} Vt}{2} \tag{6.59}$$

where

$$<\rho_t> = \frac{1}{t}\int_t \rho(x)\mathrm{d}x$$

The extrapolation to $r = 0$ is more accurate the larger the ratio of $2R/t$.

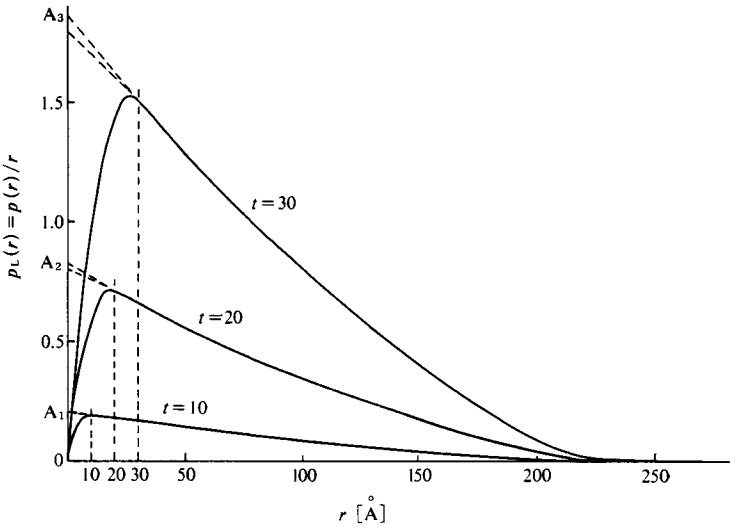

Fig. 6.13 Functions of lamellar particles with the same plane (100 × 100) and varying thickness t (10, 20, 30). The transition points are signalized by the vertical dashed lines.[21]
[Reproduced with permission from I. Pilz *et al.*, *Methods in Enzymology*, **61**, 170, Academic Press (1980)]

Figure 6.14 gives a comparison of $p(r)$ and $p_L(r)$ between a sphere, a prolate ellipsoid and an oblate ellipsoid having the same number of excess electrons and radius of gyration.

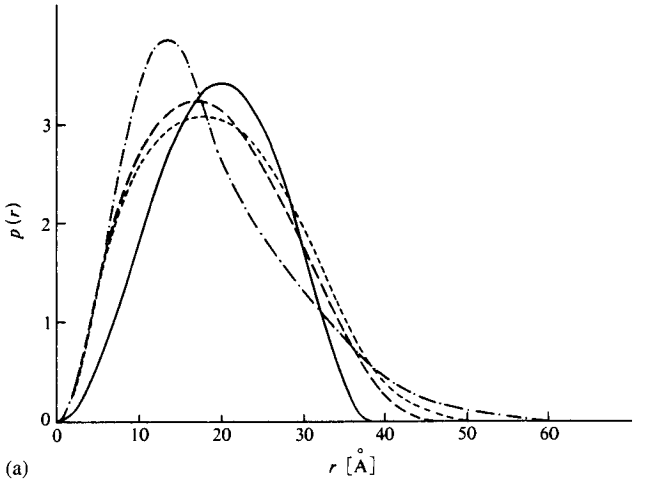

Fig. 6.14 Comparison of the distance distribution functions of a sphere (——), a prolate ellipsoid of revolution 1 : 1 : 3 (—·—·—), an oblate ellipsoid of revolution 1 : 1 : 0.2 (----) and a flat prism 1 : 1 : 0.23 (---) with the same radius of gyration. (a): $p(r)$ function.

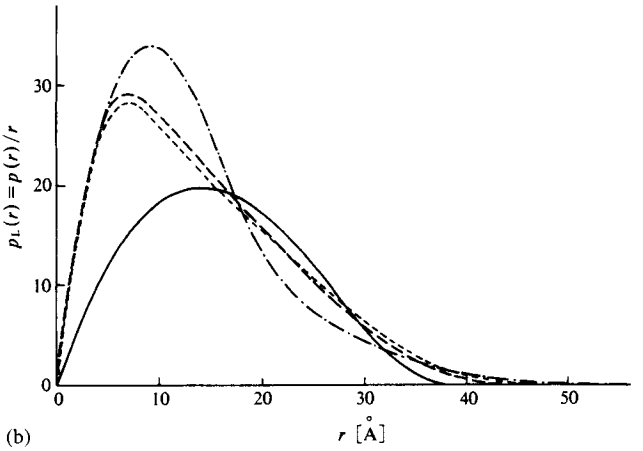

Fig. 6.14 (*Continued*)
(b); $p_L(r)$ function.[21]
[Reproduced with permission from I. Pilz *et al.*, *Methods in Enzymology*, **61**, 171, Academic Press (1980)]

C. Distance distribution function and radius of gyration and zero angle intensity

The radius of gyration of the particle, R_g, mentioned earlier is defined by the distance distribution function, $p(r)$,

$$R_g^2 = \frac{\int p(r)r^2 dr}{2\int p(r)dr} \tag{6.60}$$

and the scattering intensity at zero angle, $I(0)$, is a constant: 4π times the integral of the $p(r)$:

$$I(0) = 4\pi \int p(r)dr \tag{6.61}$$

D. The scattering intensity and the distance distribution function

The relation between the scattering intensity and distance distribution of a particle is given by the Fourier transformation

$$I(S) = 4\pi \int \gamma(r) \frac{\sin 2\pi Sr}{2\pi Sr} dr = 4\pi \int p(r) \frac{\sin 2\pi Sr}{2\pi Sr} dr \tag{6.62}$$

The corresponding relation between the scattering amplitude $A(S)$ and the radial electron density distribution $\rho(r)$ of a centrosymmetrical particle is given by

$$A(S) = 4\pi \int \rho(r)r^2 \frac{\sin 2\pi Sr}{2\pi Sr} dr \tag{6.63}$$

Inverse transformation gives

$$\gamma(r) = 4\pi \int I(S) S^2 \frac{\sin 2\pi Sr}{2\pi Sr} \mathrm{d}S \tag{6.64}$$

or

$$p(r) = 2 \int I(S) \cdot Sr \cdot \sin(2\pi Sr) \mathrm{d}S \tag{6.65}$$

and from Eq. 6.63

$$\rho(r) = 4\pi \int A(S) \cdot S^2 \frac{\sin 2\pi Sr}{2\pi Sr} \mathrm{d}S \tag{6.66}$$

6.2.4 Polydispersed system of particles with uniform shape

When the shape is uniform but there is a distribution of particle diameters we may take $M(R_g)$ as the mass distribution function of particles between R_g and $R_g + \mathrm{d}R_g$, and the scattering intensity will be given by

$$I = K_0 \int_0^\infty M(R_g) {R_g}^3 \exp(-s^2 {R_g}^3/3) \mathrm{d}R_g \tag{6.67}$$

If this particle size distribution is approximately divided into N rectangular distributions and the ratio of the weight of the particles in the jth component to the total particle weight is $W(R_{gj})$, then

$$\begin{aligned} I &= K_0 \sum_{j=1}^{N} W(R_{gj}) {R_{gj}}^3 \exp(-s^2 {R_{gj}}^3/3) \\ &= K_0 \sum_{j=1}^{N} W(R_{gj}) {R_{gj}}^3 \exp\{-(4\pi^2/3\lambda^2)\varepsilon^2 {R_{gj}}^2\} \end{aligned} \tag{6.68}$$

In practice, a tangent drawn to the lower end of the log I *vs.* ε^2 curve (*cf.* Fig. 13.22) gives R_{g1}, the minimum radius of gyration. The radius of gyration R_{g2} of the second component is found by subtracting the intensity corresponding to this tangent from the original curve and drawing a tangent to the curve produced in this way. Successive repetitions of this operation give R_{g1}, R_{g2}, R_{g3},... The weight ratios $W(R_{gj})$ of the size fractions can then be found from the ratios of the intercepts of the tangents on the ordinate $K_j = K_0 W(R_{gj}) {R_{gj}}^3$, the Jellinek-Solomon-Fankuchen method.[25]

The subject of errors due to the slit system and their elimination is covered in Section 15.1.2. Correction in the case of the Guinier plot is, however, very simple. For measurements made with a slit that is so narrow and long that it can be considered as approximating a slit of infinite height and zero width, calculation of I_H from Eq. 6.68 and 15.2 gives

$$\begin{aligned} I_H &= K_0 \sum_{j=1}^{N} W_j(R_{gj}) {R_{gj}}^3 \int_0^\infty \exp\{(-4\pi^2/3\lambda^2)(\varepsilon^2 + t^2/r^2) {R_{gj}}^2\} \mathrm{d}t \\ &= K_0' \sum_{j=1}^{N} W_j(R_{gj}) {R_{gj}}^2 \exp\{(-4\pi^2/3\lambda^2)\varepsilon^2 {R_{gj}}^2\} \end{aligned} \tag{6.69}$$

Accordingly, since the gradient of the Guinier plot for each component is not affected by the slit height, R_{gj}, may be calculated directly from Eq. 15.5. Since the value of the intercept is $K_j' = K_0' W_j(R_{gj}) {R_{gj}}^2$, as shown by Eq. 6.69 if the weight ratio is calculated using $W_j {R_{gj}}^2$ in place of $W_j {R_{gj}}^3$, the correct result is obtained without correction for the effect of errors caused by the slit.[26]

A very convenient formula is given by Hosemann,[27] if $M(R_g)$ is a Maxwellian,

$$M(R_g)=\left(\frac{R_g}{R}\right)^n \exp\left\{-\left(\frac{R_g}{R}\right)^2\right\}\frac{2}{R\Gamma\left(\frac{n+1}{2}\right)} \tag{6.70}$$

$\Gamma\left(\frac{n+1}{2}\right) \cong \left(\frac{n-1}{2}\right)!$ is the Γ-function. The weight averaged particle radius $< R_g >$ and the polydispersity g_R are given by

$$< R_g >= R\Gamma\left(\frac{n+3}{2}\right)\Big/\Gamma\left(\frac{n+1}{2}\right) \cong R(n+1)/(2n+3)^{\frac{1}{2}} \tag{6.71}$$

$$g_R=\frac{(< R_g{}^2 > - < R_g >^2)^{\frac{1}{2}}}{< R_g >}=\left[\frac{\Gamma\left(\frac{n+5}{2}\right)\Gamma\left(\frac{n+1}{2}\right)}{\left\{\Gamma\left(\frac{n+3}{2}\right)\right\}^2}\right]^{\frac{1}{2}} \cong \{2(n+1)\}^{\frac{1}{2}} \tag{6.72}$$

The intensity is given by

$$I = I_e\, Mn^2[1+(sR_g)^2/3]^{-(n+4)/2} \tag{6.73}$$

For small g_R, hence $n > 100$ it reduces to the Guinier equation (Eq. 15.4).

6.2.5 Small-angle scattering from systems of densely packed particles

If particles producing small-angle scattering are sufficiently densely packed we must consider not only the interference contributed by individual particles, but also the mutual interference between neighboring particles, just as the mutual interference between neighboring atoms had to be taken into account in extending the treatment of the X-ray diffraction by monatomic gases to the case of liquids. Since the scattering amplitude for one particle is $(\Psi)^{1/2}$, the system may be treated as a densely packed assembly of hypothetical atoms having scattering factors $(\Psi)^{1/2}$, and the composite scattering amplitude may be found by the method of Section 2.5. The scattering theory for a monatomic liquid cannot, however, be applied without modification. The details of the treatment will not be given here, but small particles differ from atoms in that their size and shape are not constant. Moreover, the regular cohesive forces which exist between atoms (Van der Waals forces, etc.) lead to fairly regular statistical distributions of neighboring atoms, whereas the cohesive forces between small particles differ with their nature and external shape, so that the statistical distributions of such systems are rather complex. Thus there are very few cases in which the theory of X-ray scattering for liquids is strictly applicable, and special care is generally necessary in the interpretation of small-angle scattering from densely packed particles.

The following is a brief description of the main points of scattering theories for densely packed systems of particles with certain specific shapes.

A. Spheres of uniform size

In the scattering Eq. 2.28, derived initially by Zernicke and Prins[28] and by Debye and Menke[29] for monatomic liquids, replacement of the atomic scattering factor f by the number of electrons n in one article and the scattering function, $\Psi(s)$, for a sphere (see again Table 5 of the Appendix) gives

$$I(S) = I_e Mn^2 \Upsilon(s)^2\left\{1+\int_0^\infty 4\pi r^2[\rho(r)-\rho_0]\frac{\sin sr}{sr}\mathrm{d}r\right\} \tag{6.74}$$

ρ_0 is the average particle density in the system and $\rho(r)$ is the particle density in the immediate environment of a particle. It should be noted that Eq. 6.74 is of the same form as Eq. 2.28, with the scattering intensity Ψ for a single spherical particle in place of the square of atomic scattering factor, f^2.

If the radial particle density distribution $P(r)$ is zero for $0 < r < R$ and constant for $r > R$ (the case with Fig. 2.16(a)), the value for intensity given by Eq. 6.74 is dependent upon the particle density, since particle density $\rho(r) = P(r)/v$. The effect is such that interference increases with increasing particle density, but approximates more closely to single particle scattering as the density decreases. This is shown in Fig. 6.15. The dependence does not change in character even if the scattering body is rod-shaped or lamellar rather than spherical.

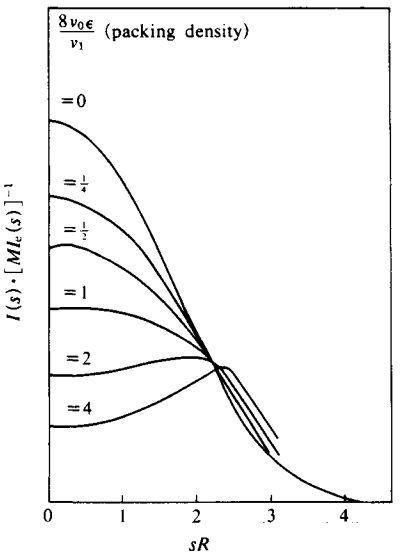

Fig. 6.15 Theoretical scattering curves for rigid spherical particles having various packing densities ($sR = 2\pi S\,R = 2\pi\varepsilon R/\lambda$).[5]
[Reproduced from A. Guinier, G. Fournet, *Small-Angle Scattering of X-Rays*, p.50, John Wiley & Sons, Inc. (1955)]

Fournet[30] has also derived a general equation, but based on a rather different approach. Lund and Vineyard[31] have calculated the scattering intensity for clusters of several spherical particles.

B. Spheres and ellipsoids of revolution of different sizes

Fournet[12] calculated the scattering intensity for dense assemblies of spheres having two different radii, and Kratky and Porod[9] and Hosemann[27] calculated intensities for dense assemblies of spheres whose radii have a Maxwellian distribution.

Roess and Shull[32] calculated the scattering by an ensemble of ellipsoids of revolution.

C. Dense accumulations of lamellae

Kratky and Porod[9] calculated the intensity for this case as a model of the structure of the crystalline regions in natural and synthetic fibers. In this case neither the thickness of the

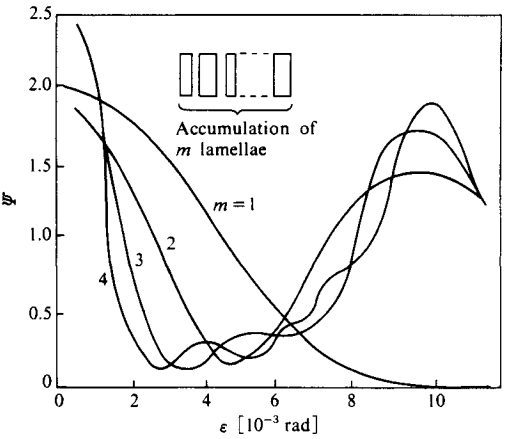

Fig. 6.16 Influence of m on the scattering curve for lamellar packing.[9] [Reproduced from O. Kratky, G. Porod, *J. Colloid Sci.*, **4**, 35, Academic Press (1949)]

lamellae nor the distance between them is constant. Various analyses all give scattering curves with a maximum in the same position despite differences in the statistical treatment of the thickness variation, as shown in Fig. 6.16.[9] This maximum can be interpreted as corresponding to the position of the Bragg diffraction (Eq. 4.1) for the average distance between the layers in the crystalline region. Kratky and Porod extended the theory further and carried out numerous investigations on the structure of fibers. Section 13.6.3 gives more details of techniques, results, etc.

D. Parallel bundles of long cylinders

This theory, which is applicable to cellulose fibrils, was developed, and the calculations performed, by Kratky and Porod[9] using the same statistical methods as in **C** above.

6.2.6 Small-angle scattering from a non-particulate system

A. Scattering power and invariant

If we write the electron density $\rho(r)$ of an inhomogeneous system (volume V) as

$$\rho(r) = <\rho(r)> + \Delta\rho(r), \tag{6.75}$$

where $<\rho(r)>$ is the average electron density of the system and $\Delta\rho(r)$ is fluctuation of the electron density. The scattering amplitude of the system is

$$S(S) = \int <\rho(r)> \exp[2\pi i(\boldsymbol{S}\cdot\boldsymbol{r})]\mathrm{d}v_r + \int \Delta\rho(r)\exp[2\pi i(\boldsymbol{S}\cdot\boldsymbol{r})]\mathrm{d}v_r \tag{6.76}$$

In an ordinary case, the first term in the right side can be neglected in the very neighborhood of $Sr = 0$, and if $r = r_2 - r_1$

$$S(S) = \int \Delta\rho(r_1)\exp[-2\pi i(\boldsymbol{S}\cdot\boldsymbol{r}_1)]\mathrm{d}v_{r1} \int \Delta\rho(r_2)\exp[2\pi i(\boldsymbol{S}\cdot\boldsymbol{r}_2)]\mathrm{d}v_{r2}$$

$$= \iint_{(\mathbf{r}=r_2-r_1)} \Delta\rho(r_1+r)\exp[2\pi i(\boldsymbol{S}\cdot\boldsymbol{r})\mathrm{d}v_{r1}]\mathrm{d}v_r \tag{6.77}$$

Let

$$Q(r) = \int \Delta\rho(r_1)\Delta\rho(r_1+r)\mathrm{d}v_{r1} \tag{6.78}$$

then

$$I(S) = \int Q(r)\exp[2\pi i(\boldsymbol{S}\cdot\boldsymbol{r})]\mathrm{d}v_r \tag{6.79}$$

or inversely

$$Q(r) = \int I(S)\exp[-2\pi i(\boldsymbol{S}\cdot\boldsymbol{r})]\mathrm{d}v_s \tag{6.80}$$

If $r = 0$ in Eqs. 6.78 and 6.80

$$\frac{1}{V}Q(0) = \frac{1}{V}\int(\Delta\rho(r_j))^2\mathrm{d}v_j = <(\Delta\rho(r))^2> = \frac{1}{V}\int I(S)\mathrm{d}v_s \tag{6.81}$$

Eq. 6.81 shows that the mean square deviation of the electron density $<(\Delta\rho(r))^2>$ is equal to the total scattering intensity per unit volume. This may be called the "scattering power"of the system.

For isotropic scattering the right side of Eq. 6.81 may be written as

$$Q(0) = 4\pi\int_0^\infty S^2 I(S)\mathrm{d}S \tag{6.82}$$

This type of integral scattering intensity has been termed the "invariant".[19]

The volume of the particle can be determined, using the Q and $I(0)$, the scattering intensity at zero angle, as

$$V = I(0)/Q \tag{6.83}$$

For the two-phase system, in which ρ_1 and χ_1 are the electron density and the volume fraction of the disperse phase (or solute), respectively, and ρ_2 and χ_2 $(= 1 - \chi_1)$ those of dispersant (solvent), respectively.

$$(\rho_1 - \rho_2)^2\chi_1\chi_2 = (\Delta\rho)^2\chi_1\chi_2 = <(\Delta\rho)^2> \tag{6.84}$$

Substituting this into Eq. 6.81

$$(\rho_1 - \rho_2)^2\chi_1\chi_2 = Q(0)/V \tag{6.85}$$

This can be applied to the crystallinity (volume) measurement of the system consisting of crystalline and amorphous regions by means of X-ray small-angle scattering.

B. Correlation function and specific internal surface

The correlation function[22,23] (or characteristic function[19–21]), $\gamma(r)$ mentioned before (Section 6.2.3A) can be written as follows using the Q and $Q(0)$.

$$\gamma(r) = \frac{Q(r)}{Q(0)} = \frac{\int I(S)\exp[2\pi i(\boldsymbol{S}\cdot\boldsymbol{r})]\mathrm{d}v_s}{\int I(S)\mathrm{d}v_s} \tag{6.86}$$

In a randomly distributed two-phase system, for electron densities ρ_1 and ρ_2, such as

holes in a solid or particles interspersed with voids, it has been shown[23] that

$$\gamma(r) = \exp[-r/< l_c >], \tag{6.87}$$

and

$$\frac{O}{V} = \frac{4\chi_1\chi_2}{< l_c >} \tag{6.88}$$

The term O/V is the specific internal surface defined in terms of the overall volume of the system, V. l_c is the correlation length (or distance) or reduced inhomogeneity length,[19,33] a measure of the size of inhomogeneities, which gives the integral breadth of $\gamma(r)$. If we define the transversal, or inhomogeneity, lengths l_1 and l_2 as given below,

$$< l_1 > = \frac{4\chi_1}{O/V} \quad \text{and} \quad < l_2 > = \frac{4\chi_2}{O/V} \tag{6.89}$$

by comparison with Eq. 6.44 it can be written as

$$\frac{1}{< l_c >} = \frac{1}{< l_1 >} + \frac{1}{< l_2 >} \tag{6.90}$$

According to Kratky and coworkers, the $< l_1 >$ and $< l_2 >$ can be visualized as follows.[34] If we imagine the system to be pierced in all directions at random by rays (Fig. 6.17), the mean length of all the line segments intercepted. by the disperse phase is $< l_1 >$ whereas the mean length of all the segments intercepted by the dispersant is $< l_2 >$.

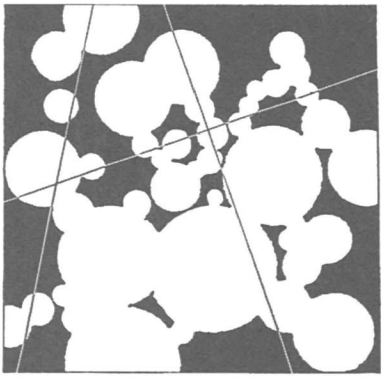

Fig. 6.17 Transversal or inhomogeneity length.[43] [Reproduced with permission from O. Kratky, *Angew Chem.*, **72**, 478, Verlag Chemie (1960)]

The theory of small-angle scattering has been presented in outline. For further details the reader is referred to other books on the subject.[5,10a),16,18,35–43] Experimental methods and applications will be described in later chapters.

References

1. A. Guinier, *Ann. Phys. (Paris)*, **12**, 161 (1939).
2. O. Kratky, *Naturwissenschaften*, **26**, 94 (1938).
3. R. Hosemann, Z. *Physik*, **113**, 759 (1938); *ibid.*, **114**, 133 (1939).
4. M. Kakudo, in: *X-Ray Crystallography* (I. Nitta ed.), Vol. II, p. 519, Maruzen (1961).
5. A. Guinier, G. Fournet, *Small-Angle Scattering of X-Rays*, p. 201, John Wiley & Sons, Inc., N.Y. (1955).
6. T. Seto, in: *Structure and Physical Properties of High Polymers*, Vol. II. pp. 307–319 Baifukan, Tokyo (1973).
7. Lord Rayleigh, *Proc. Roy. Soc., (London)*, **A90**, 219 (1914).
8. In ref. 5, p. 20.
9. O. Kratky, G. Porod, *J. Colloid. Sci.*, **4**, 35 (1949).
10. a) In ref. 9, p. 20.
    b) *International Tables for X-Ray Crystallography*, Vol. III, pp. 324–326, Kynoch Press, Birmingham (1968).
11. D. L. Dexter, *Phys. Rev.*, **90**, 1007, (Serial approximation) (1953).
12. G. Fournet, *Doctoral Thesis*, Paris Univ., series A. No. 3256, 2384 (1950).
13. *International Tables for X-Ray Crystallography*, Vol. III, 327, Kynoch Press, Birmingham (1968).
14. H.M. Barton, R. Brill, *J. Appl. Phys.*, **21**, 783 (1950).
15. a) H. Stuhrmann, Z. *Phys. (Frankfurt am Main)* [*N.S.*], **72** (1970).
    b) H. Stuhrmann, *J. Appl. Cryst.*, **7**, 173 (1974).
    c) K. Ibel, H. Stuhrmann, *J. Mol. Biol.*, **93**, 255 (1975).
    d) H. Stuhrmann, A. Miller. *J. Appl. Cryst.*, **11**, 325 (1978).
16. I. Pilz, O. Glatter, O. Kratky, *Methods in Enzymology*, **61**, 180, Academic Press, N.Y. (1980).
17. H. Stuhrmann, in: *Small-angle X-ray Scattering*, (O. Glatter, O.Kratky eds.) p.197, Academic Press, N.Y. (1982).
18. C.R. Cantor, P.R. Schimmel, *Biophysical Chemistry*, Part II, Techniques for the Study of Biological Structure and Function, p. 831, W.H. Freeman, San Francisco (1980).
19. G. Porod, *Kolloid-Z.*, **124**, 83 (1951); *ibid.*, **125**, 51 (1952).
20. G. Porod, *Acta Phys. Austriaca*, **3**, 255 (1948).
21. a) In ref. 16, pp. 152–167.
    b) O. Glatter, O. Kratky eds., *Small Angle X-ray Scattering*, pp.167–196, Academic Press, London (1982).
22. P. Debye, A.M. Bueche, *J. Appl. Phys.*, **20**, 518 (1949).
23. P. Debye, H.R. Anderson, H. Brumberger, *J. Appl. Phys.*, **28**, 679 (1957).
24. In ref. 16, pp. 167–180.
25. M.H. Jellinek, E. Solomon, I. Frankuchen, *Ind. Eng. Chem.*, **18**. 172 (1946).
26. M. Kakudo, N. Kasai, M. Kimura, Y. Kubota, T. Watase, *J. Chem. Soc. Jpn., Pure Chem. Sect.* (in Japanese), **78**, 821 (1957); N. Kasai, M. Kakudo, T. Watase, *Technol. Rept. Osaka Univ.*, **8**, 433 (1958).
27. R. Hosemann, *Kolloid-Z.*, **117**, 13 (1950).
28. F. Zernike, J.A. Prins, Z. *Physik*, **41**, 184 (1927).
29. P. Debye, H. Menke, *Ergeb. Tech. Röntgenkunde*, **2**, 1 (1931).
30. G. Fournet, *Acta. Cryst.*, **4**, 293 (1950).
31. L.H. Lund, G.H. Vineyard, *J. Appl. Phys.*, **20**, 593 (1949).
32. L.C. Roess, C.G. Shull, *J. Appl. Phys.*, **18**, 308 (1947).
33. L. Kahovec, G. Porod, H. Ruck, *Kolloid-Z*, **133**, 16 (1953).
34. O. Kratky, *Pure and Appl. Chem.*, **12**, 483 (1966).
35. R. Hosemann, S.N. Bagchi, *Direct Analysis of Diffraction by Matter*, North-Holland, Amsterdam (1962).
36. V. Luzzati, *Small-angle X-Ray Scattering on an Absolute Scale*, (H.H. Pattee, V.E. Coslett eds.) and A. Engström, *X-Ray Optics and X-Ray Microanalysis*, Academic Press, N.Y. (1963).
37. W.O. Statton: *Small-angle X-Ray Studies of Polymers in Newer Methods of Polymer Characterization, Handbook of X-Rays* (B. Kaelbe ed.), Interscience, N.Y. (1963).
38. *Small-angle Scattering* (H. Brumberger ed.), Gordon & Breach, Reading (1967).
39. L.E. Alexander, *X-Ray Diffraction Methods in Polymer Science*, Wiley-Interscience, N.Y. (1969).
40. J. Schelten, R.W. Hendricks, *J. Appl. Cryst.*, **11**, 297 (1978).
41. H.B. Stuhrmann, A. Miller, *J. Appl. Cryst.*, **11**, 325 (1978).
42. O. Glatter, X-ray techniques and, Neutron techniques in: Small-angle techniques, in: *International Tables for Crystallography* Vol. C, (A.J.C. Wilson ed.), Kluwer Academic Pub., Dordrecht (1992).
43. O. Kratky, *Angew. Chem.*, **72**, 478 (1960).